ACS APPLIED MATERIALS & INTERFACES

Research Article

www.acsami.org

Manufacture of Void-Free Electrospun Polymer Nanofiber Composites with Optimized Mechanical Properties

Urszula Stachewicz,[†] Farid Modaresifar,[‡] Russell J. Bailey,[‡] Ton Peijs,[†,‡] and Asa H. Barber*[,†,‡]

[†]Nanoforce Technology Ltd. and [‡]Department of Materials, School of Engineering and Materials Science, Queen Mary University of London, Mile End Road, London E1 4NS, United Kingdom

Supporting Information

ABSTRACT: Engineered fiber reinforced polymer composites require effective impregnation of polymer matrix within the fibers to form coherent interfaces. In this work, we investigated solution interactions with electrospun fiber mats for the manufacture of nanocomposites with optimized mechanical properties. Void free composites of electrospun nonwoven PA6 nanofibers were manufactured using a PVA matrix that is introduced into the nonwoven mat using a solution-based processing method. The highest failure stress of the composites was reported for an optimum 16 wt % of PVA in solution, indicating the removal of voids in the composite as the PVA solution both impregnates the nanofiber network and fills all the pores of the network with PVA matrix upon evaporation of the solvent. These processing methods are effective for achieving coherent nanofiber−matrix interfaces, with further functionality demonstrated for optically transparent electrospun nanofiber composites.

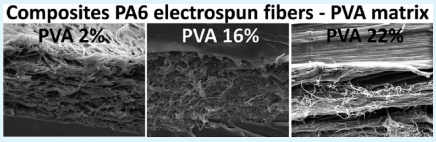

KEYWORDS: *nylon 6, PVA, composite, mechanical properties, electrospinning*

INTRODUCTION

Electrospun nanofibers are used increasingly as a reinforcement phase in fiber reinforced polymer nanocomposites. These electrospun fibers have been effective in reinforcing rubber films,[1] increasing the strength and stiffness of an epoxy matrix,[2] and delivering reinforcement in hard nanodiamond-polymer composites.[3] The mechanical performance of electrospun nanocomposites is critically dependent on a coherent interface being formed between the electrospun fiber acting as the reinforcement and the surrounding polymer matrix that binds the fibers together. Manufacturing of electrospun fiber−polymer nanocomposites therefore requires effective impregnation of the electrospun fiber mat with polymer matrix so that an intimate contact is created between fiber and matrix phases. Engineered fiber reinforced polymer composites often suffer from poor impregnation during manufacture, which results in voids.[4] These voids within composite structures lead to stress concentration points during external loading and result in relatively poor composite mechanical properties.[4,5] Previous work has highlighted wetting of organic solvents with electrospun fiber surfaces,[6] which would suggest that polymer solutions containing a matrix material can effectively impregnate electrospun fiber mats and remove void formation at the fiber-matrix interface, to provide effective composite mechanical properties. Indeed, a number of works have used matrix solution impregnation as an effective technique to impregnate electrospun fiber mats to produce composite material structures.[1,7,8]

The spreading of a liquid phase within a solid fiber mat of electrospun fibers is defined by a number of parameters including the surface free energy of the liquid and solid, porosity of the solid and the viscosity of the liquid phase. The tuning of the liquid phase viscosity for complete coverage within a solid porous structure is typically described using Washburn theory.[9] Solution processing of electrospun fiber composites can therefore potentially be described using Washburn theory and is critical in directing the optimization of solution viscosity for complete coverage of the porous electrospun fiber structures. A void-free composite of matrix binding reinforcing electrospun fibers will result after solvent evaporation from the impregnating solution. Poor solution impregnation within the electrospun fiber mat leads to void formation upon solvent evaporation, poor stress transfer and enhanced stress-concentration sites during external loading of the composite, and consequently, ineffective mechanical performance.[10] Such optimization of solution-based processing has been significant in the production of nanofiber composites, most notably for carbon nanotube reinforcements, where wetting of nanotubes with polymer solutions produced enhanced composite properties.[11,12] However, direct correlation between mechanical performance of fiber nanocomposites and the optimization of solution-based processing has not been developed for electrospun fiber materials or, indeed, for other nanofibrous materials such as carbon nanotubes.

In this study, we investigate solution interactions with electrospun nanofiber mats for the manufacture of nanocomposites with optimized mechanical properties. The concepts developed in this work are generic and are applicable for the manufacture of a potentially diverse range of nanofibers bound together within polymer matrices processed from

Received: February 10, 2012
Accepted: April 23, 2012
Published: April 23, 2012

   dx.doi.org/10.1021/am300235r | ACS Appl. Mater. Interfaces 2012, 4, 2577−2582

solution impregnation. While a number of polymers have been electrospun successfully, we use here electrospun nylon 6 (PA6) nonwoven nanofibers and polyvinyl alcohol (PVA) as a matrix. PA6 has been previously shown to be both a mechanically effective electrospun nanofiber material[13,14] with polar liquids spreading over the fiber surfaces.[6] PVA is therefore a potentially effective model matrix due to its solubility in polar solvents and has been successfully incorporated as a polymer matrix for nanotube and nanorod composites.[15] Mechanical evaluation of the resultant composite structures will be used to assess the PVA solution impregnation within the PA6 nanofiber mats and highlight the ability to optimize nanofiber composite manufacture.

MATERIALS AND METHODS

Polyamide 6 (PA6, M_w = 24 000 g mol^{-1}, BASF, Ultramid B33 L, Germany) was dissolved in a mixture of acetic acid (≥99.7%, Sigma Aldrich, U.S.A.) and formic acid (98%, Sigma Aldrich, U.S.A.) (50/50 mass ratio) to produce a resultant polymer concentration of 12 wt % in solution. The PA6 polymer solution was electrospun into nanofibers using a large scale multi-jet electrospinning setup (NanoSpider, Elmarco, Czech Republic) as used in our previous studies.[6,14] The electrospun nanofiber diameter was 134 ± 44.31 nm as measured using scanning electron microscopy (SEM, Inspect F, FEI Company, U.S.A./E.U.). An example of a nonwoven PA6 nanofiber mat is presented in Figure 1. Strips with a width, W, and length, L, of 10 mm ×80 mm were cut from the collected nanofiber mat using a sharp blade. The electrospun polymer strips were weighed to give a mass of nanofibers, m_{nf}, within the strip. The density of nanofibers within the strip was found using a gas pycnometer (AccuPyc 1330 He, U.S.A.) with the average nanofiber density ρ_{nf} found to be 1.29 g.cm^{-3}. The thickness, t, of the electrospun nanofiber strip samples were measured using a micrometer and found to vary from 0.05 to 0.12 mm. We attempted to avoid micrometer compression of the sample where possible by visual inspection of the sample. The total volume of the strip, V_c, is equal to the sum of the volume of electrospun nanofibers V_{nf} and the volume of voids between the nanofibers, V_v. As the total volume of the strip $V_c = WLt$ and the volume of nanofibers $V_{nf} = \rho_{nf}/m_{nf}$, the porosity P_c in the nanofiber strip is given as the volume fraction V_v/V_c and can be written fully as $P_c = 1 - (\rho_{nf}/m_{nf})/WLt$. The porosity of five electrospun nanofiber strips was measured to give an average porosity of 0.88 ± 0.025.

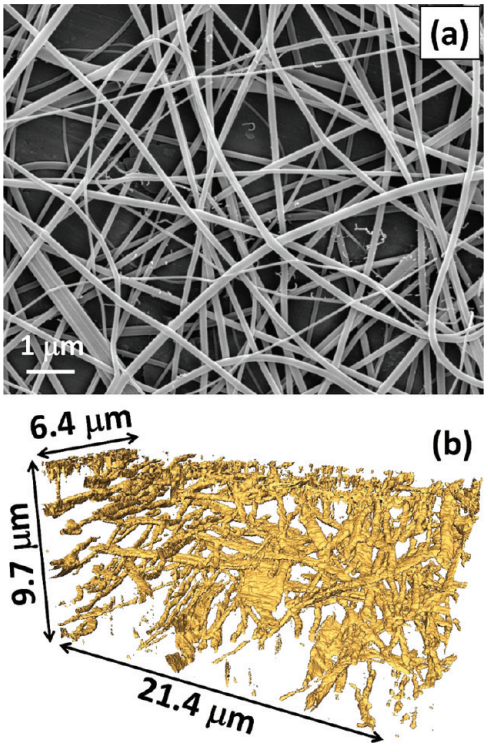

Figure 1. (a) Scanning electron micrograph of electrospun PA6 nanofibers and (b) 3D reconstruction of the electrospun PA6 nanofiber network.

Visualization of the electrospun nanofiber strip to measure the pore diameter directly was achieved using 3D Focused Ion Beam (FIB) tomography using a small dual beam (SDB) microscope (Quanta 3D FEG, FEI Company, E.U./U.S.A.) and following previous protocols.[16] The SDB allows both imaging of surfaces with SEM and removal of the surface layer using FIB to allow further SEM imaging. Collection of 2D SEM images as the FIB mills through samples is used for subsequent 3D reconstruction. Nanofiber strips were first wetted with aqueous iodine solution for image contrast and flash frozen under liquid nitrogen. The flash frozen iodine solution ensured that the voids within the nanofiber mat were filled with amorphous solid so that the cross-section surface, and not the out of plane structures within the pores of the nanofiber mat, was imaged with the SEM. The frozen nanofiber strips were coated with platinum and transferred to the cryo-stage of the SDB so that the top surface was perpendicular to the electron beam direction. The sample stage was tilted within the SDB so that the sample surface was perpendicular to the FIB direction and the electron beam had an angle of incidence of 52°. The cryo-stage was maintained at a temperature of −130 °C. Following the protocol described by Bushby et al.,[16] a volume of material (40 μm × 50 μm × 30 μm) at a site on the sample surface was milled away using the FIB, and a side trench (10 μm × 40 μm × 30 μm) was milled at either side of the site of interest. The proceeding material was removed in order to provide an unobstructed view of the material cross-section and, together with the side trenches, prevented a buildup of redeposited material near the site of interest. Cross-sectional slices of 50 nm were milled using FIB from the block of the nanofiber sample at 30 kV and a final beam current of 0.5 nA. The collected images were filtered and converted to black and white using Image J (version 1.44p, NIH, U.S.A.) to improve the contrast between the nanofibers and solid amorphous water for the mat reconstruction. The 3D reconstruction of the nanofiber sample was obtained using Resolve RT (version 5.2 – FEI Edition, Germany), as shown in Figure 1b. The average area fraction occupied by electrospun nanofibers was calculated for each slice used in the 3D reconstruction using particle analysis in ImageJ and gave values of V_{nf} = 0.04 and V_v = 0.96. The average distance between fibers giving the void diameter, assuming uniform distribution between nanofibers, is 1.69 μm. The porosity calculated based on 3D reconstruction is higher than the porosity of 0.88 measured previously using density measurements. This difference is expected to be due to the image processing of the 3D reconstruction as the collected images require filtering to obtain necessary contrast between fibers and the background. This image processing, depending on the defined threshold of the filter, can lead to increased spacing between fibers and consequently increased porosity values.

Composites were prepared by impregnating the electrospun PA6 strips with solutions of PVA. Polyvinyl alcohol (PVA, M_w = 85 000–124 000 g mol^{-1}, density ρ_{PVA} = 1.269 g cm^{-3}, Sigma Aldrich, U.S.A.) was first dissolved in distilled water at 80 °C to produce 2, 4, 6, 8, 10, 14, 16, 18, 20, and 22 wt.% solution concentrations. Higher concentrations of PVA solution were not possible due to saturation. The viscosity of the PVA solution was measured using a rheometer (AR Rheometer, TA Instruments, U.S.A.) and the solution surface tension found using a Drop Shape Analysis System (Krüs, DSA100, Germany). Nanofiber strips were submerged into 20 mL of PVA solution of differing concentrations contained in a glass Petri dish as shown in Figure 2. The electrospun nanofiber strips were held in PVA solution for 24 h, which caused both uptake of the solution into the strips and evaporation of solvent to leave solid PVA within the void spaces between the electrospun nanofibers. The strips containing solid PVA were subsequently removed from the Petri dish for mechanical

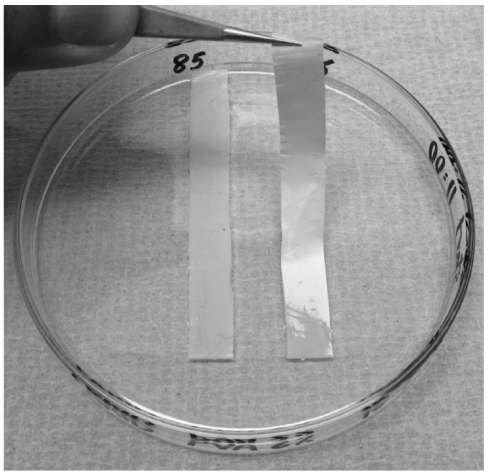

Figure 2. Optical photograph showing the production of nanocomposites by submerging nanofiber strips into PVA solutions.

testing. The weight increase of the electrospun nanofiber strips was therefore assigned to the addition of PVA within the voids of the strips as shown in Table 1.

Table 1. PVA Availability for Uptake in Impregnation of Electrospun PA6 Nanofiber Mats for Composite Preparation

PVA solution concentration (%)	mass of PVA uptake during nanofiber mats impregnation (g)	mass of PVA required for filling up 88.4% porosity (g)	difference between uptake and required mass of PVA (g)
2	0.0408	0.0722 ± 0.0257	−0.0314
4	0.0815		0.0093
6	0.1223		0.0501
8	0.1631		0.0909
10	0.2038		0.1316
14	0.2854		0.2132
16	0.3261		0.2539
18	0.3669		0.2947
20	0.4076		0.3354
22	0.4484		0.3762

Quasi-static tensile testing of nanofiber strips and their composites to failure was performed using an Instron Universal Testing Machine (Instron 5566, U.K.) with a 1 kN load cell (Instron, U.K.). The composite strain ε was calculated from $\Delta L/L_o$, where ΔL is the sample extension and L_o is the original sample length. Optical extensometers were used during nanofiber tensile testing for accurate strain measurements. The stress, σ, was calculated from the applied force F, dividing by the effective cross-sectional area of nanofibers from the nanofiber volume fraction V_{nf}, as evaluated by gas pycnometry.

Failed fracture surfaces of representative samples of each electrospun nanofiber-PVA composite were investigated using scanning electron microscopy (SEM) with an accelerating voltage of 10 kV and a working distance of 8−10 mm. Carbon cement was applied at the edges of the samples to provide a conductive path from the top of the fracture surface to the conductive stage. Additional sample conduction was achieved by sputter coating with gold for 30 s (Agar Auto Sputter Coater, U.K.) to give a thin (<10 nm) conducting layer.

RESULTS AND DISCUSSION

Mechanical Considerations. The impregnation of the PVA solution within the electrospun nanofiber mat is correlated with the corresponding solution viscosity. Figure 3 shows an increase in the PVA solution viscosity as the concentration of PVA increases in the solution. This figure indicates that the

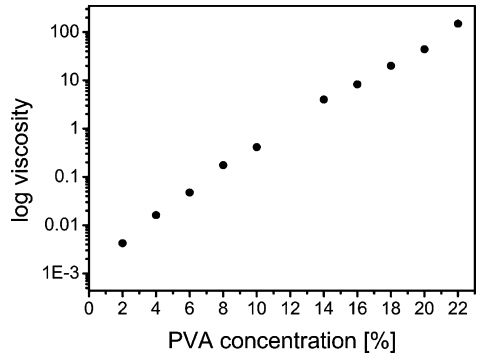

Figure 3. Plot of the increase in polymer solution viscosity with increasing wt % PVA in solution. The insert highlights the viscosity increase for the lower PVA concentrations in solution shown in the main plot.

time required for the polymer solution to spread over the nanofiber surfaces will increase as the solution concentration increases. However, an increased solution viscosity denotes a capacity for more PVA uptake into the pores of the electrospun nanofiber mats during the solution processing of the composite. The plot of decreasing solvent evaporation rate with increasing PVA concentrations in Figure 4 suggests that although higher

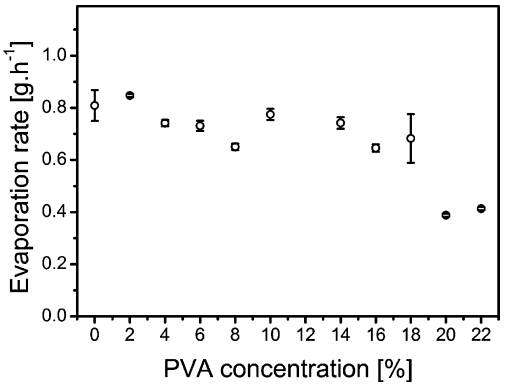

Figure 4. Plot of the water evaporation rate for a range of PVA concentrations in solution.

viscosity solutions have less mobility than the lower solution viscosities, the time available for the higher viscosity solutions to flow within the pores of the nanofiber mat increases because of the slower removal of water from the solution. The optimization of solution viscosity to deliver PVA to within the voids of the nanofiber mat and the time available to achieve this can be correlated to mechanical testing. In particular, low viscosity solution impregnation within the electrospun nanofiber mat may occur readily but evaporation of solvent will cause a relatively small volume fraction of PVA within the voids of the mat. Further, a relatively high viscosity solution will have insufficient time to spread throughout the nanofiber mat and cause some voids to remain unfilled within the PVA. These voids lead to poor fiber−matrix stress transfer and are stress concentration sites that promote failure within the composite during tensile testing.

A typical example of the stress−strain behavior of a nanofiber-PVA composite relative to the base materials of electrospun PA6 nanofiber mats and a homogeneous PVA polymer film is shown in Figure 5. The average tensile stress for PA6 nanofiber mats of 44.2 ± 5.06 MPa (see the Supporting

dx.doi.org/10.1021/am300235r | ACS Appl. Mater. Interfaces 2012, 4, 2577−2582

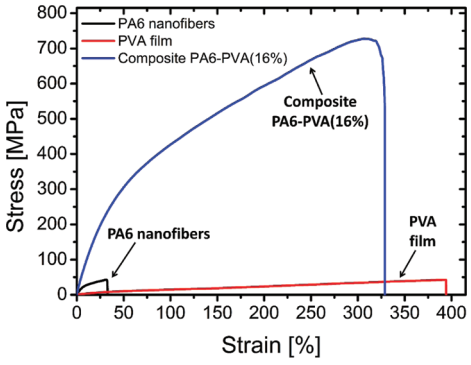

Figure 5. Examples of stress–strain curves obtained from tensile testing of electrospun PA6 nanofibers, PVA film and PA6–PVA matrix composites prepared with 16 wt % PVA solution concentration.

Information, Figure 1Sa and Table S1) is consistent with previous results.[14] The apparent cross section used in calculations of stress in composites reinforced with fibers follows established standards.[17] Specifically, the applied force is assumed to act over the effective cross-sectional fiber area defined as the volume fraction in order to determine the apparent stress in the composite. This apparent stress ignores the stresses acting in the PVA matrix and void contribution, but is suitable in highlighting the efficiency of the fiber reinforcement. An increase in the apparent failure stress of the composite is therefore an indication of the increased efficiency of fiber reinforcement in the composite. This improved reinforcement efficiency is due to impregnation of PVA within the porosity of the fibers that improves stress transfer between fibers. Therefore, we are able compare the mechanical properties of nanofibers with and without the matrix. The failure strain of the nanofiber-PVA composite can be recorded from these stress–strain curves and is shown for composites prepared with a range of different PVA solutions as indicated in Figure 6a. The recorded failure strain of the nanofiber-PVA composites is shown to increase in Figure 6b with increasing PVA concentration in solution. However, poor impregnation of PVA within the voids of the nanofiber network will still cause deformation of the PVA and, as the failure strain of the PVA fiber mat is larger than PA6 (see the Supporting Information, Figures S1 and S2 and Table SI), the overall composite failure strain will continue to increase as more PVA is added to the composite with increasing PVA concentration. The composite strain is therefore somewhat restrictive in determining PVA impregnation. The stress in the composite is more difficult to define as the applied force during tensile testing is required to act over the cross-sectional area of the sample. Thus, an established standard[17] is used to determine the apparent failure stress and define the reinforcing efficiency of the electrospun nanofibers in the composite. The composite cross-section consists of electrospun nanofibers, PVA matrix and voids. Potentially poor impregnation of the PVA solution into the electrospun nanofiber mats or large amounts of solvent evaporating for low PVA concentrations in solution will cause a significant amount of void spaces in the cross-section. Therefore, we calculate an apparent failure stress in the composite by assuming that the stress is acting over the nanofiber cross-sectional area only as previously defined.[17] The force applied to fail the composite will act over an increasing cross-sectional area as the voids between the nanofibers are filled with PVA. A correspondingly larger force is required to

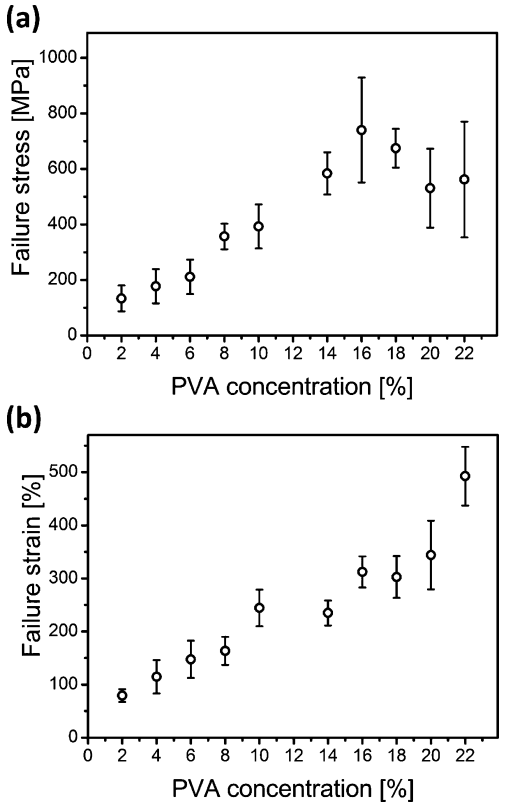

Figure 6. Plots of (a) the electrospun PA6-PVA composite apparent failure stress and (b) failure strain for composites prepared with PVA solutions of differing concentrations.

fail the composite and, as we assume the cross-sectional area is fixed for the nanofiber contribution only, an increase in the apparent failure stress occurs. The filling of voids within the electrospun nanofiber mats will therefore cause an increase in the apparent failure stress. A plot of the apparent stress increase with increasing PVA concentration in solution is shown in Figure 6 and conforms to the mechanism of voids within the electrospun nanofiber mat being progressively filled with PVA. However, a drop in the apparent failure stress occurs when using PVA solution concentrations of 20 wt % and greater. Observation of the nanofiber-PVA composite fracture surfaces in Figure 7 indicate a decrease in the void frequency up to 20 wt % of PVA but then shows a further increase in the void density at the highest PVA concentrations used. The drop in the apparent failure stress of the composite at the higher PVA concentrations in solution would support the mechanism of a high viscosity solution requiring a relatively large time to impregnate the nanofiber mat and, as the solvent is evaporating, the PVA becomes solid before complete impregnation occurs. The optimized PVA concentration in solution for impregnation within the electrospun PA6 nanofiber mats is therefore 16 wt %.

Porosity Considerations. According to the modeling work of Mao and Russell, capillary wicking phenomena in nonwoven fibrous structures occurs along the direction of fiber orientation and depends on porosity, fiber diameter and orientation.[18] The phenomenological mechanism proposed for the filling of voids within the fiber mat is based on the spreading process dominated by viscous and inertial forces. Fluid flow in the porous media is time dependent and can be described by Washburn's law.[9] If the liquid penetrates a distance L through

dx.doi.org/10.1021/am300235r | ACS Appl. Mater. Interfaces 2012, 4, 2577–2582

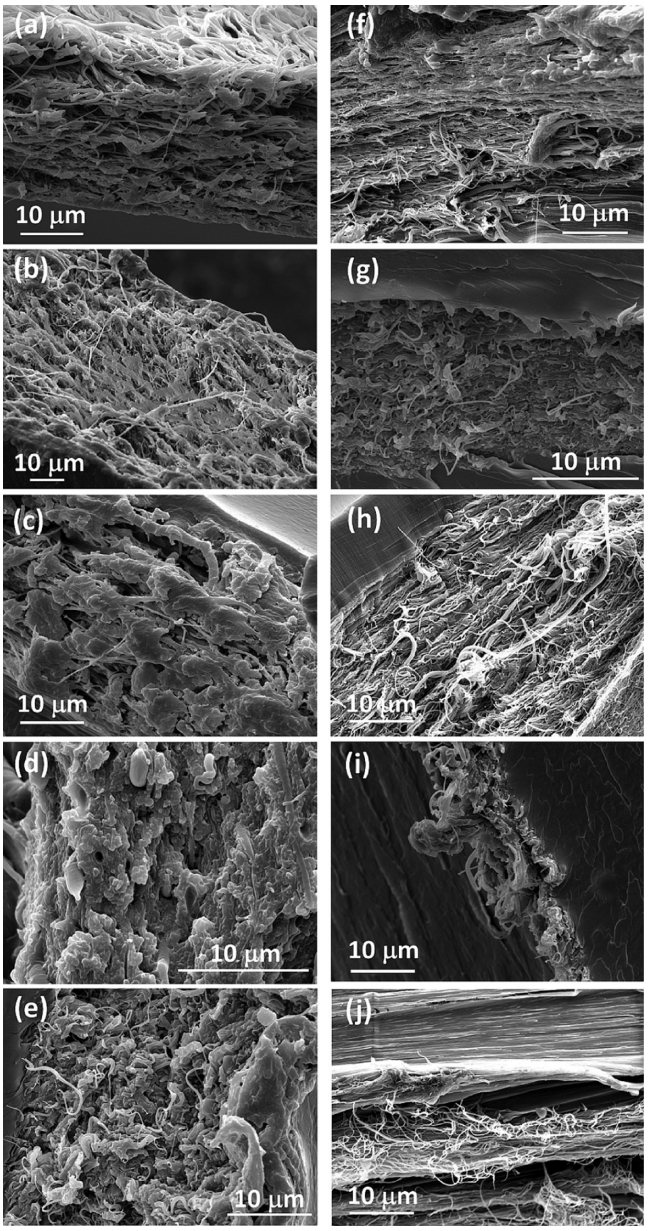

Figure 7. Scanning electron micrographs of nanocomposite fracture surfaces after tensile testing for composites prepared with PVA solution concentrations of (a) 2, (b) 4, (c) 6, (d) 8, (e) 10, (f) 14, (g) 16, (h) 18, (i) 20, and (j) 22 wt %.

the pores of a material in a time T, the material's pore diameter D is given by

$$L^2 = \frac{\gamma D T}{4\eta} \tag{1}$$

where γ is the surface tension and η is the dynamic viscosity of the PVA solution used to impregnate the electrospun nanofiber mat. A 16 wt % PVA solution is chosen for pore diameter calculation using Washburn's law due to the solution impregnation exhibiting the highest apparent failure stress indicated in Figure 6 and Figure 7g. The viscosity of the 16 wt % PVA solution, taken from Figure 3, is 8.25 ± 0.87 Pa·s and a surface tension of 54.9 mN m^{-1}. Following Washburn's consideration we are able to determine the pore size of nonwoven mats from the time dependent flow. To calculate the average pore diameter D of nanofiber mats, we measured the PVA 16 wt % solution penetration distance, L, within the electrospun nanofiber mat change over time by optical microscope (Olympus BX 60 with Digital Imaging, Japan) as shown in Figure 8. The penetration of solution was measured

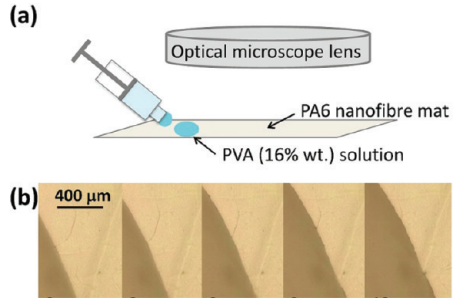

Figure 8. (a) Schematic setup of PVA wetting the nanofiber network (b) Optical microscope images showing the progression, from left to right, of PVA 16% solution flow in the PA6 nanofiber network, taken at 3 s time intervals.

from optical images using Image Pro-Express (version 5.0.1.26, Media Cybernetics, Inc. U.S.A.). Because the spreading of the solution was not uniform, the penetration distance was measured at 3 or more points in each image taken every 3 s. The average value of all measured points was used in the calculations of pore diameter in nanofiber mats. The measurement of liquid spreading in nonwoven nanofiber mats gives us the average pore size calculated using eq 1 of 1.13 ± 0.21 μm, which is a comparable result to the 3D reconstruction of a nanofiber network, where the average pore diameter was estimated at 1.6 ± 0.32 μm. The pore sizes calculated from eq 1 for 16 wt % PVA solution and from 3D image are in the same range indicating full impregnation of porous nanofibers mats.

Increasing the viscosity of PVA solution used for nanofiber impregnation controls the flow of the solution into porous media. As the solution becomes more viscous, the viscous drag opposing the PVA uptake was higher for PVA solutions with higher concentration, reaching the point when the PVA matrix did not penetrate the whole nanofiber mat, which can be seen in the case of the 20 and 22 wt % PVA solutions. Kinetic viscosity also contributes to mass transport, for example, in 2 wt % PVA, there is not enough polymer material to be transported into the nanofiber network, and therefore, insufficient impregnation of nanofiber mats occurs.

Additional justification of void free composites is typically made by consideration of the transparency of nanocomposite samples.[19] Fewer voids is represented by a transparency increase, Figure 9, where an increased concentration of PVA used in solution led to more PVA trapped in the porous nanofiber and better optical transparency. The transparency of the composite films starts to decrease for composites using PVA concentration of 20 wt % and higher. Moreover, the theoretical effect of porosity on material strength can be calculated with the following equation[10,20]

$$\sigma_p = \sigma_d(1 - V_p)^2 \tag{2}$$

where σ_d and σ_p are tensile stress for fully dense and porous material respectively, and V_p is pores volume fraction. Assuming the fully dense composite is prepared with a optimum PVA concentration of 16 wt %, the average tensile failure stress, σ_d (for V_p =0) is 740 MPa and knowing the average, σ_p for each

dx.doi.org/10.1021/am300235r | ACS Appl. Mater. Interfaces 2012, 4, 2577−2582

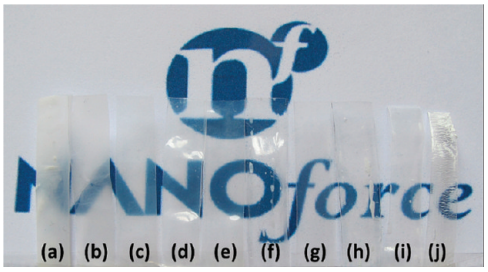

Figure 9. Optical photograph showing transparency of PA6-PVA composites with different PVA concentrations of (a) 2, (b) 4, (c) 6, (d) 8, (e) 10, (f) 14, (g) 16, (h) 18, (i) 20, and (j) 22% wt.

composite (see supporting material, Table SI) we can calculate the theoretical porosity (V_p) for each of the other composites. The results presented in Figure 10, calculated from the tensile

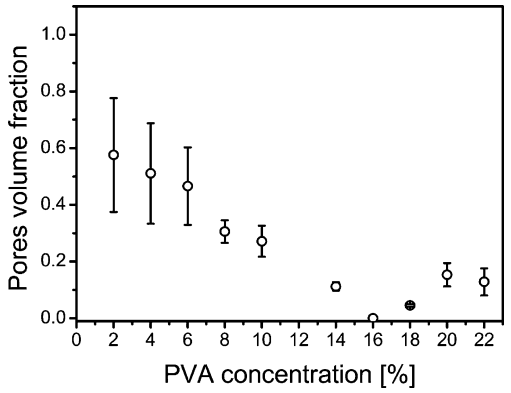

Figure 10. Plot of the electrospun PA6–PVA composite theoretical porosity volume fraction for composites prepared with PVA solution of differing concentrations. Error for the pores volume fraction is calculated based on the error in the average tensile failure stress for the composite.

testing data, confirm the observations from SEM imaging that the porosity within the composites decreases with increasing PVA concentration. As the mechanical performance of composites depends on composite porosity, a significant increase in tensile strength is observed for composites with pore volume fraction below 0.2.

CONCLUSIONS

Void free composites of nonwoven PA6 nanofibers bound by a PVA matrix introduced into the nonwoven fibers were produced using a solution-based processing method. The highest failure stress of the composite was found for an optimum PVA solution of 16 wt %, which indicated the effective removal of void formation in the composite as the PVA solution both impregnates throughout the nanofiber network and fills the pores of the network completely with PVA upon evaporation of the solvent.

ASSOCIATED CONTENT

Supporting Information

Load–extension and stress–strain curves obtained from tensile testing of electrospun PA6 nanofiber mats, PVA film and all PA6 nanofiber–PVA matrix composites together with a table summarizing average tensile stress and tensile strain values (PDF). This material is available free of charge via the Internet at http://pubs.acs.org

AUTHOR INFORMATION

Corresponding Author

*E-mail: a.h.barber@qmul.ac.uk.

Notes

The authors declare no competing financial interest.

ACKNOWLEDGMENTS

We thank Dr Zofia Luklinska at the Queen Mary NanoVision Centre for assistance with microscopy facilities.

REFERENCES

(1) Kim, J. S.; Reneker, D. H. *Polym. Compos.* **1999**, *20*, 124–131.
(2) Lin, S.; Cai, Q.; Ji, J. Y.; Sui, G.; Yu, Y. H.; Yang, X. P.; Ma, Q.; Wei, Y.; Deng, X. L. *Compos. Sci. Technol.* **2008**, *68*, 3322–3329.
(3) Behler, K. D.; Stravato, A.; Mochalin, V.; Korneva, G.; Yushin, G.; Gogotsi, Y. *ACS Nano* **2009**, *3*, 363–369.
(4) Wang, S. Z.; Adanur, S.; Jang, B. Z. *Compos., Part B* **1997**, *28*, 215–231.
(5) Jeong, H. *J. Compos. Mater.* **1997**, *31*, 276–292.
(6) Stachewicz, U.; Barber, A. H. *Langmuir* **2011**, *27*, 3024–3029.
(7) Romo-Uribe, A.; Arizmendi, L.; Romero-Guzman, M. E.; Sepulveda-Guzman, S.; Cruz-Silvan, R. *ACS Appl. Mater. Interfaces* **2009**, *1*, 2502–2508.
(8) Eichhorn, S. J.; Dufresne, A.; Aranguren, M.; Marcovich, N. E.; Capadona, J. R.; Rowan, S. J.; Weder, C.; Thielemans, W.; Roman, M.; Renneckar, S.; Gindl, W.; Veigel, S.; Keckes, J.; Yano, H.; Abe, K.; Nogi, M.; Nakagaito, A. N.; Mangalam, A.; Simonsen, J.; Benight, A. S.; Bismarck, A.; Berglund, L. A.; Peijs, T. *J. Mater. Sci.* **2010**, *45*, 1–33.
(9) Washburn, E. W. *Phys. Rev.* **1921**, *17*, 273.
(10) Patel, H. K.; Ren, G.; Hogg, P. J.; Peijs, T. *Plast. Rubber Compos.* **2010**, *39*, 268–276.
(11) Raravikar, N. R.; Schadler, L. S.; Vijayaraghavan, A.; Zhao, Y. P.; Wei, B. Q.; Ajayan, P. M. *Chem. Mater.* **2005**, *17*, 974–983.
(12) Ma, J.; Deng, H.; Peijs, T. *Macromol. Mater. Eng.* **2010**, *295*, 566–574.
(13) Hang, F.; Lu, D.; Bailey, R. J.; Jimenez-Palomar, I.; Stachewicz, U.; Cortes-Ballesteros, B.; Davies, M.; Zech, M.; Boedefeld, C.; Barber, A. H. *Nanotechnology* **2011**, *22*, 365708.
(14) Stachewicz, U.; Peker, I.; Tu, W.; Barber, A. H. *ACS Appl. Mater. Interfaces* **2011**, *3*, 1991–1996.
(15) Zhang, Z.; Wan, M. *Synth. Met.* **2002**, *128*, 83–89.
(16) Bushby, A. J.; P'ng, K. M. Y.; Young, R. D.; Pinali, C.; Knupp, C.; Quantock, A. J. *Nat. Prot.* **2011**, *6*, 845–858.
(17) *ASTM Standard D2343-09 : Test Method for Tensile Properties of Glass Fiber Strands, Yarns, and Rovings Used in Reinforced Plastics*; ASTM International: West Conshohocken, PA, 2009.
(18) Mao, N.; Russell, S. J. *J. Appl. Phys.* **2008**, 104.
(19) Gea, S.; Bilotti, E.; Reynolds, C. T.; Soykeabkeaw, N.; Peijs, T. *Mater. Lett.* **2010**, *64*, 901–904.
(20) Mackenzie, J. K. *Proc. Phys. Soc. B* **1950**, *63*, 2.